University of Glasgow

James Watt School of Engineering

ENG 5026: Design Special Topic 5

Laser Auto-Alignment for Communication Systems in the Developing World.

Report Written By:
Kyle Watt,
Rory Mullen,
Tamim Abdul Maleque

2024/25

Supervisors: Professor Martin Lavery, Adam Vallance, Mark Main

Acknowledgment

We would like to extend our gratitude to Mark Main, Adam Vallance for their continuous support with technical support and laboratory guidance. We are also grateful to Professor Martin Lavery for the advice of the project and for allowing us to use the facilities of his Structured Photonics Group.

Abstract

In this DST project, the development and evaluation of a compact, low-cost motorised auto-alignment platform for free-space optical communication (FSOC) system was designed to mitigate the effects of temperature and pressure fluctuations that impact the optical alignment of the fibres in the FSO system. A mechanical assembly done using 3D-printed PLA, which includes ~~a~~ X-Y flexure controlled a lead-screw mechanisms (which have a 0.20 mm pitch, hence a minimal step size of approximately 0.666 µm per rotation) using the, by the off-the-shelf 28BYJ-48 stepper motors and A4988 drivers for a automated alignment. A mechanical design connecting the Z-axis alignment with XY flexure was done using 3D-designed and printed runners, which also operated using ~~a~~ lead-screw mechanisms and used a cheap threaded steel 4-inch driveshaft. A purpose ~~purpose~~-designed PCB was done where the Raspberry Pi Pico 2350 B microcontroller used a raster and spiral scan algorithm-based control to search and find the optimum power level. The raster and spiral algorithms were tested both to great success, with both scanning over areas with both high and low optical power before settling on the peak. This project shows that each of the algorithms is far superior to manual control at identifying and aligning the FSOC system with more precision.

Contents

Introduction

The internet is a vital need to billions of people in the world. Internet access fosters economic growth, security and technological developments in digital technology & artificial intelligence [1]. However, there is a stark digital divide globally, with an estimated 2.6 billion people remaining unconnected according to the 2023 press release article by International Telecommunication Union [2]. This divide affects developing nations because of the limitations of infrastructure and associated costs in deployment of traditional fibre optic cables, in geographically challenging or sparsely populated rural areas. As highlighted in the discussion on tackling Africa's digital divide, the capital cost of fibre can go upwards of US$100,000 per kilometre, which creates an economic barrier due to initial fibre infrastructure establishment [3].

Furthermore, even when deployed, fibres in remote regions can be susceptible to damage from environmental factors or theft, hence increasing the barriers for socio-economic progress. This limitation of connectivity necessitates the use and development of cost-effective alternative technologies to bridge the digital divide, using Free Space Optical Communication (FSOC).

Free Space Optical Communication (FSOC) transmits data through the atmosphere using beams of light, typically in the infrared (IR) spectrum, which is an alternative to traditional cabled solutions [3]. Conceptualised as ‘fibre optics without the fibre’ FSOC offers the potential for gigabits per second (Gbps) data rates [4]. This high capacity is due to the vast, typically unregulated bandwidth available at optical frequencies (Near IR region wavelengths: 850nm, 1310nm, and 1550nm). Therefore, the optical spectrum offers bandwidths that are orders of potentially tens of terahertz (THz) across various windows if compared to entire radio frequency (RF) spectrum, where individual services are allocated bandwidth typically measured in megahertz (MHz) or gigahertz (GHz). The RF spectrum is also often licensed by regulatory bodies.

The theoretical upper bound on the information rate that can be transmitted over a communication channel is given by the Shannon-Hartley theorem, which states that the channel capacity (C), in bits per second, is $C=B \times \log_2(1+S/N)$, where B is the bandwidth of the channel in hertz, S is the average received signal power, and N is the average noise power [5].Increasing bandwidth can increase channel capacity although not limitless as the relationship between signal to noise ratio is a constraint and other practical limitations such as power, dispersion and system integration need to be considered.

Recognising the potential of FSOC, the practical deployment of the systems is met with operational challenges. A primary concern, once an initial line-of-sight is established, is the maintenance of precise optical alignment between the transmitter and receiver [6]. The stability of this alignment is important for maintaining link performance, as very

small deviations can lead to significant signal loss or complete link failure, especially as distance between transceivers increase. But, how are these issues arising? FSOC systems are susceptible to mechanical misalignments from sources such as thermal changes of mounting structures due to daily and seasonal temperature fluctuations, wind effects on buildings or structures where the equipment is housed and mechanical vibrations present in the physical world [4].

Narrow beam divergence which is inherent in laser-based communication makes precise pointing accuracy extremely important for FSOC. Pointing accuracy requirements can be on the order of several hundred microradians. Atmospheric effects such as turbulence (causing signal scintillation and beam wander) and attenuation due to fog or haze also impact long distance FSOC performance [4][6]. These atmospheric phenomena can cause the laser beam's intensity to fluctuate unpredictably, its path to deviate from the direct line-of-sight, and its overall power to diminish significantly before reaching the receiver, all of which degrade the quality and reliability of the communication link

Previously, for the FSOC set-up at University of Johannesburg, correcting such fine misalignments has required manual intervention, delicate screw adjustments using costly high-precision commercial components (Thorlabs XY Translation Mounts – costing approximately £170 each). This reliance on manual recalibration not only increases operational expenditure but also introduces delays in restoring connectivity, which impacts accessibility and scalability of FSOC solutions, especially in resource-limited settings.

To address the solution of mechanical misalignment and reduce costly manual recalibration in FSOC systems, this project focused on developing an entirely 3D printed compact, motorised auto-alignment system for XYZ axis. Using Commercial Off-The-Shelf (COTS) components to create the system accessible, affordable and easily replicable solution would hence democratise access to stable FSOC systems.

Primary tasks of the auto-alignment use precise motorised control (using stepper motors), for fine adjustments. Such a system will operate in three axes:

- **X-Y Adjustment**: Provides angular correction crucial for coupling light into optical fibres (often with core diameters around 100µm).
- **Z-Axis Adjustment**: Optimises beam focus or collimation, vital for maximising received signal power, especially over longer distances where beam divergence is a factor.

The auto-alignment system is algorithm-based, that uses search patterns to locate and optimise the optical signal. Two common algorithms used in auto-alignment solution are **Raster Scanning and Spiral Scanning** [7] as depicted in Figure 1 below. Raster

Scanning is often one of the quickest methods for initially finding the beam at the receiver ("first light"). It operates by scanning along one axis (x-axis) and then indexing by a certain distance along another (y-axis), repeating this cycle. The advantage in this method is the utility for finding the threshold power detection (above -25dBm) and for subsequent search to find peak power optimisation. This method is limited to two-axis operation and involves discrete start-stop motions.

An additional method of Spiral Scanning executes an outward spiral motion, where it too can be used to find the first light in a larger general area of the beam and search for highest power position after completing the spiral. Continuous spiral scans offer smoother motion, where in computer programme the spiral code is described in polar coordinates (r, θ). This method is also limited to two-axis operation and requires completion of the entire trajectory described in space.

Figure 1: Illustration of search patterns used in FSO auto-alignment. (Left) Raster Scan Pattern and (Right) Spiral Scan Pattern.

The development of a cheaper and better commercially available auto-alignment solution makes FSOC a more practical as and sustainable solution for a more range of applications. For example, these portable self-aligning systems can be highly advantageous for providing emergency connectivity during disaster situations when terrestrial infrastructure is compromised [4] [6].

FSOC systems effectively address the "last mile" connectivity challenge, bridging the final network gap to end-users where fibre installation is often costly and complex [3][4]. Compared to fibre, deploying FSOC transceivers on existing structures like rooftops is less complex, and they can be integrated into hybrid communication networks with RF or fibre links to enhance overall reliability [3] [4]. These advantages enable rapid FSOC deployment, providing high-speed digital links to remote and rural communities while overcoming obstacles related to terrain, installation costs, infrastructure security and so bridging the digital divide [3] [4].

While transient obstructions might cause brief interruptions, the high bandwidth of FSOC links and multiple channels can mitigate the impact on many common internet activities. The deployment of such enabling technology also aligns strongly with several United Nations Sustainable Development Goals (UN SDGs), by fostering economic growth (UNSDG 8), promoting innovation and infrastructure (UNSDG 9), and reducing inequalities (UNSDG 10).

Project Management

As a three-member team, communication was facilitated through MS Teams and WhatsApp, with a primary emphasis on in-person meetings. Work delegation was a collaborative effort, involving regular communication and consultation with supervisors, Mark and Adam.

Recognising the importance of early prototyping, the team initiated this process alongside printed circuit board (PCB) design. Electronic components were sourced with a focus on cost-effectiveness and global availability.

The Structured Photonics Group's laboratory's 3D printing facilities were utilised for rapid prototyping and assembly of the mechanical system, enabling iterative testing and refinement. Algorithm work was completed in parallel with PCB design, ensuring that GPIO pins and electronic requirements were matched. The work was then performed in an optics laboratory on an optical table for testing of the full mechanical system with the algorithm written. A flowchart of the full process in this project is shown in figure 2 below.

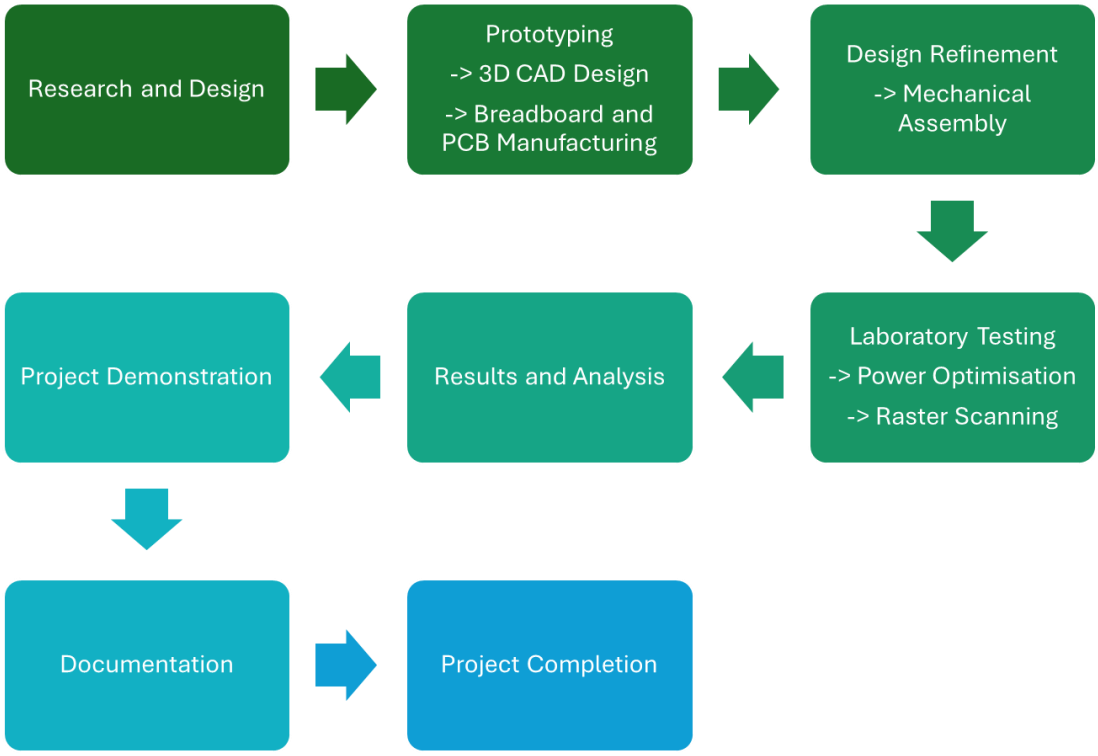

Figure 2: The Design Build and Test Project Flowchart of this project.

While the project successfully met its primary objectives, an area for improvement in project management would have been to maintain a more consistent pace of progress throughout the semester.

PCB Design

Requirements and Justification

The PCB was one of the earliest components developed in this project, based on the advice that manufacturing and debugging would require as much time as possible. A custom PCB was essential, as the project aimed to control four optical fibres' X, Y, and Z movements, requiring 12 motors. Without a PCB, the system would be significantly less compact, more challenging to assemble and maintain, and more prone to errors due to increased wiring complexity.
Additionally, designing a PCB made the system more reproducible. If successful, this design could be easily replicated and deployed by communities, providing them with internet access at a low cost and greater control over how that access is delivered.

Components selection

One of the key criteria in selecting components for the PCB was ensuring that they were widely available and low-cost. This would make the design easily reproducible and affordable, allowing deployment in areas that cannot support the cost of traditional high-speed communication infrastructure.

Motor Driver

The first components selected were the motor drivers. We chose the A4988 stepper motor driver [8] because it was inexpensive (under £1) and readily available—both critical requirements. However, we encountered a challenge: each A4988 has eight input pins, and with 12 stepper motors, this would require up to 96 GPIO pins on the microcontroller - an impractical number.

To address this, we decided to minimise the number of active control inputs to each A4988. Pins that did not need to change dynamically were hard-wired to either high or low. Since micro-stepping was unnecessary, the associated pins (MS1, MS2, MS3) were grounded. Additional features such as reset and sleep were also deemed unnecessary, so these active-low pins were connected to 3.3V.

The only pins connected to the microcontroller were those essential for basic operation: step, direction, and enable.

- ➔ The step and direction pins are critical for controlling motor movement.
- ➔ Although not required for motion, the enable pin was retained to allow the microcontroller to turn off motors when idle, reducing power consumption, which was a key consideration for sustainability.

Motor

The selected motor was the 28BYJ-48 5V stepper motor [9], chosen for its low cost (~£6) and wide availability, both key selection criteria. However, a challenge arose: this motor has a unipolar configuration, while the chosen driver, the A4988, is designed for bipolar stepper motors.

Unipolar motors have a centre tap on each coil, allowing current to flow in one direction per coil half, which simplifies driving but results in lower torque. In contrast, bipolar motors lack a centre tap and require current reversal through each coil, making them more complex to drive but offering higher torque and better efficiency.

To address this mismatch, the centre tap (power) wire of the 28BYJ-48 was left unconnected, effectively converting it to bipolar mode, which allows it to work with the A4988 driver.

While the 28BYJ-48 does not offer high precision, this limitation is compensated by the mechanical design, which enables step sizes as small as 0.6 µm even without micro-stepping.

Power System

The power system used a 12V Barel jack input with a backup screw terminal, to allow it to be powered by a bench power supply. The 12V was adequate to allow functionality for the A4988 Stepper Driver, as it can function with load voltages up to 35V; however, all other components required a supply of 3.3V.

This meant the power had to be stepped down from 12V to 3.3V. To do this, we used the AP1509-33SG-13. The AP1509-33SG-13 was chosen as it is a switching regulator, meaning the energy loss to heat would be minimal. The other reason for selecting the AP1509-33SG-13 was its simplicity in converting to 3.3V from 12V, as it only required two capacitors, an inductor and a Schottky diode.

Microcontroller

The microcontroller chosen for this project was the Raspberry Pi Pico 2350 B. Again, the main reason for selecting this component was its low price and wide availability. On top of the low cost and wide availability, the Pi Pico 2350 B also has the added advantage of having 80 GPIOs, which is extremely useful for our requirements of 12 motors. An extra feature beneficial with the Pi Pico 2350 B was its ability to use multicore processing. This means that multiple processes can run in parallel; therefore, if any functions need to wait, they could be run in parallel and not block other processes.

Communication/Controls

Some final components that were added to improve the ease of use and future development of the board were DIP Switches, allowing for external control of operation and modes/algorithms used. It was also decided we would add a micro-USB port to the flash firmware of the Pi Pico 2350B to allow easy communication with external devices. TVS diodes were connected to the USB data lines (D+ and D−) to clamp high-voltage spikes caused by ESD or power surges, preventing damage to the USB transceiver or microcontroller. Since USB lines are exposed and can easily accumulate static electricity (e.g. from plugging/unplugging), TVS diodes help ensure reliable operation and extend device lifespan.

Simple LEDs were also chosen to help with debugging code and hardware. Also, male headers were connected to the motor drivers and GPIO pins to allow for external communications. All the other components chosen followed the previously mentioned components' datasheets.

Schematic Design and Evaluation

The PCB was designed using KiCAD, a cross-platform and open-source electronic Design Automation Suite. The initial steps in the PCB design were to create a schematic.

RP2350B

The recommended design from the “Hardware Design with RP2350” [10] manual was followed when designing the schematic for the RP2350B, and all essential components for operation, such as the recommended oscillator and flash memory, were added following the manual. This can be seen in Figure 3 in the next page.

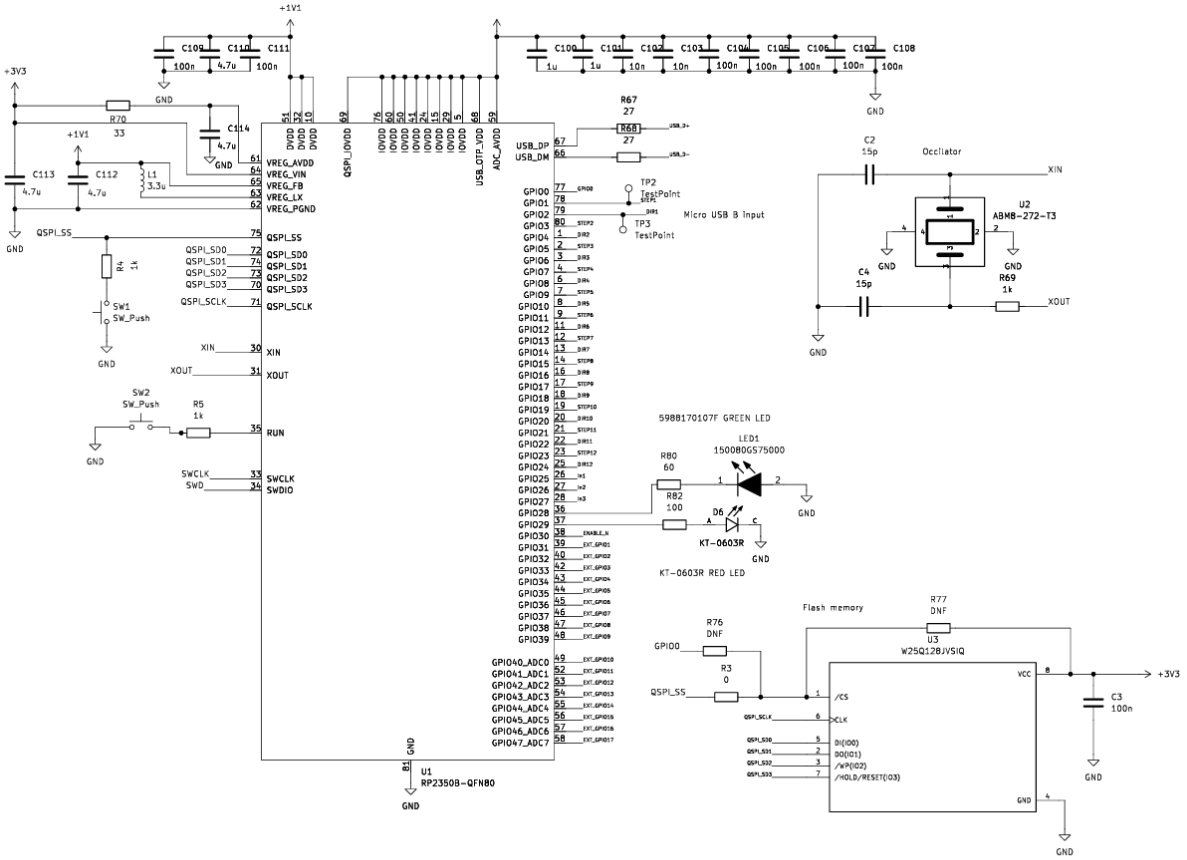

Figure 3: The 2RP2350B IC Schematic utilised in the PCB design.

As can be seen by Figure 3, the first 24 pins are used to control the step and direction of all motor drivers, and one pin, 30, is used to control the Enable function on all motor drivers. All other GPIOs were connected to allow external communication, such as buttons, LEDs and headers.

Motor Drivers

The next components are designed in the schematic, where the motor drivers are. As previously mentioned, the aim was to reduce the number of GPIO pins necessary to control the motor driver while still maintaining complete functionality. This was done by pulling all non-essential pins high or low, depending on whether they are active high or low. The A4988 was also configured to limit the maximum current to around 1 amp as higher current could potentially cause issues with the motors. This was done by configuring the reference voltage and sense resistors. In this case, the reference voltage (Vref) was 1.65V, and the sense resistors (RS), Sense 1 and Sense 2, were 0.2 Ohms.

$$Max\ Current = \frac{Vref}{8 \times RS} \approx 1Amp \qquad (1)$$

All of which can be seen in Figure 4. The outputs of the motor driver OUT1A/1B/2A/2B were all connected to a male header, allowing for easy connection to the 28BYJ-48 5V Stepper Motor.

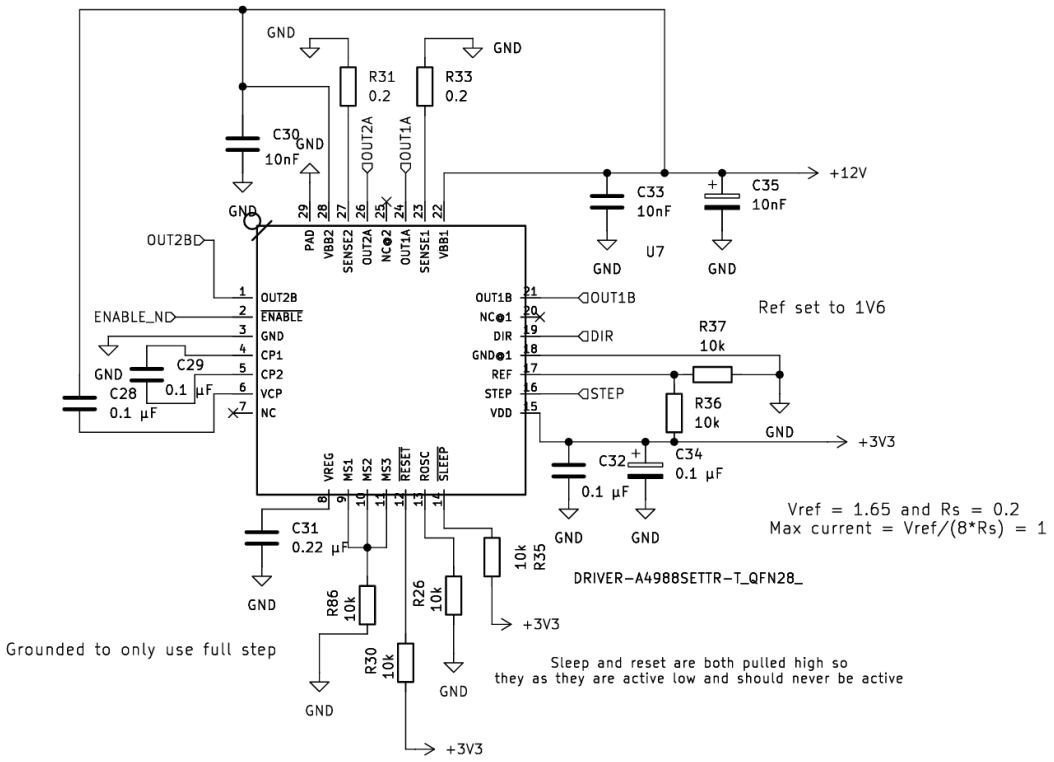

Figure 4: The Motor Driver 3 A4988 Schematic Design utilised in the PCB design.

Power

As previously mentioned, the majority of components required a 3.3V supply, and to achieve this, the AP1509-33SG-13 was used to step the power down from 12V to 3.3V. This followed the simple design outline in the AP1509-33SG-13 data sheet. However, a resistor and LED were added to indicate if the AP1509-33SG-13 was functioning as expected and producing 3.3V. Test points were also added all around the board in vital areas, such as the output from the AP1509-33SG-13, to help the debugging process. The test points were also added to other vital areas, such as the step and direction pins and the output from the A4988.

PCB Design

Board Dimensions and Stack-up

After completing the schematic, it was reviewed with the assistance of Adam Valance and Mark Main. To ensure accuracy, all design elements were carefully evaluated and cross-referenced with the component datasheets.

Once the schematic was finalised, the next step was to design the PCB. I chose a 160 mm × 80 mm board size, as there were no constraints on dimensions. This provided sufficient space to accommodate all 12 motor drivers while also ensuring adequate separation between high-EMI components like the switching regulator and sensitive data lines like the USB D+ and D-.

The PCB stack-up used signal layers on the top and bottom, with a ground plane directly beneath each to ensure low-impedance return paths and reduce ground bounce. Two power planes were used to efficiently distribute 12V and 3.3V across the board; these power planes provide a low-resistance path for power delivery and help maintain stable voltage levels across the board. The close proximity of the power and ground planes also provided beneficial inter-plane capacitance, improving high-frequency power stability and reducing noise.

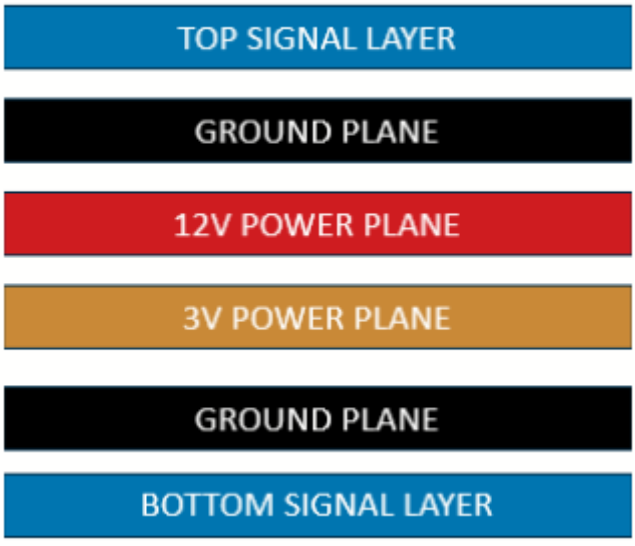

Figure 5: The 4 PCB Stack up showing the different layers of the PCB.

Component Placement

After the board had been traced out, the next step in developing the PCB was to start placing components. As previously mentioned, ensuring that components that produced a large amount of EMI were placed as far as possible from sensitive

components such as USB data lines was crucial. Therefore, the switching regulator and USB connector were placed at opposite ends of the board, as shown in Figure 6 below.

In addition to placing the switching regulator as far as possible from sensitive components to minimise electromagnetic interference (EMI), several other design choices were made to improve power integrity. One such consideration was the use of copper pours (fills) on the signal layer at the power input areas. If standard traces had been used instead of copper fill, the narrower width would have introduced higher resistance and inductance, leading to increased voltage drop and localised heating, especially under high current loads. By using copper pours, the current-carrying capacity is significantly increased, resulting in better thermal performance and reduced electrical resistance.

To connect the 12V input to the internal 12V power plane, multiple vias were used. This allowed for higher current-carrying capacity, reduced voltage drop, and improved heat dissipation. This is critical because if the via path to the 12V plane is too restricted for the required current, it can lead to localized heating, voltage instability, and in some cases contribute to increased EMI due to poor power integrity.

To further protect the power system, Schottky diodes were added at critical points. A Schottky diode was placed between the copper fill planes and the power switch, and another between the switch and the switching regulator. These diodes were chosen for their low forward voltage drop and fast switching speed, which are crucial in protecting the circuit from reverse polarity, back feeding, or inductive kickback when switching occurs. Their fast response helps clamp voltage spikes before they can propagate and damage downstream components.

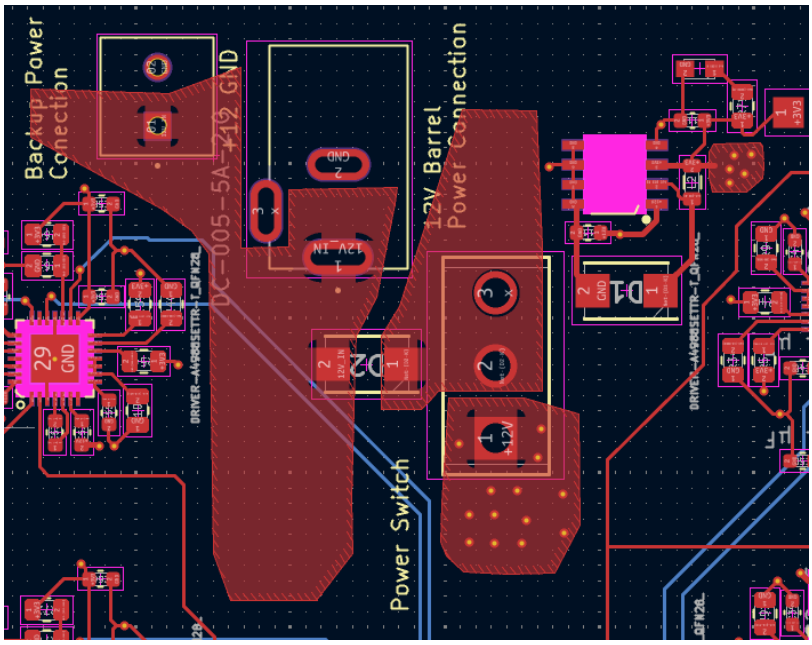

Figure 6 : The 5 PCB layout of the Power System

The stepper driver design followed the same design outlined in the schematic, only connecting vital operation pins to the GPIO of the RP2350 B. The motor driver outputs were connected to male header pins, which were labelled in a way to distinguish each optic/aperture and if it is to control the X/Y/Z for said optic, to make debugging and developing the code easier.

One key consideration when designing the motor driver layout was the placement of the decoupling capacitors. The decoupling capacitors were placed as close as possible to the power input pins of the motor driver ICs to minimise voltage ripple, suppress noise, and ensure stable power delivery during switching events. This design can be seen in Figure 7, and the same design was repeated for all 12 motor drivers.

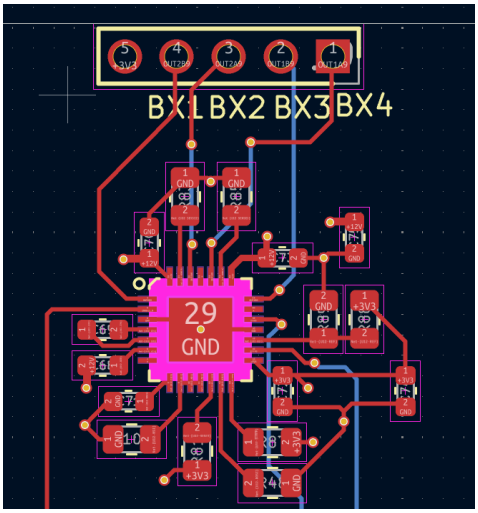

Figure 7: The 6 PCB layout of the Motor Driver

After all the motor drivers were placed and routed, the remaining key components were laid out and connected according to the schematic. One of the most challenging aspects of this stage was routing the fanout from the RP350B microcontroller. It was essential to place decoupling capacitors as close as possible to the power pins to ensure a stable voltage supply and suppress noise, as previously discussed. However, positioning them too close risked obstructing the fanout of signal traces from the adjacent GPIO and power pins.

This required an iterative layout process, carefully repositioning capacitors and adjusting trace routes to strike a balance, placing the capacitors close enough to be electrically effective while still allowing sufficient space for reliable fanout. Achieving this “sweet spot” was crucial for maintaining both signal integrity and power stability in the final design. Some other considerations were length tuning on the USB data lines. This is to ensure the data from the differential traces arrives at the same time, eliminating the chance of data corruption due to skew. Mounting holes were also

placed in the corners of the PCB, enabling possible future integration into a compact system. The full PCB design can be seen in figure 8.

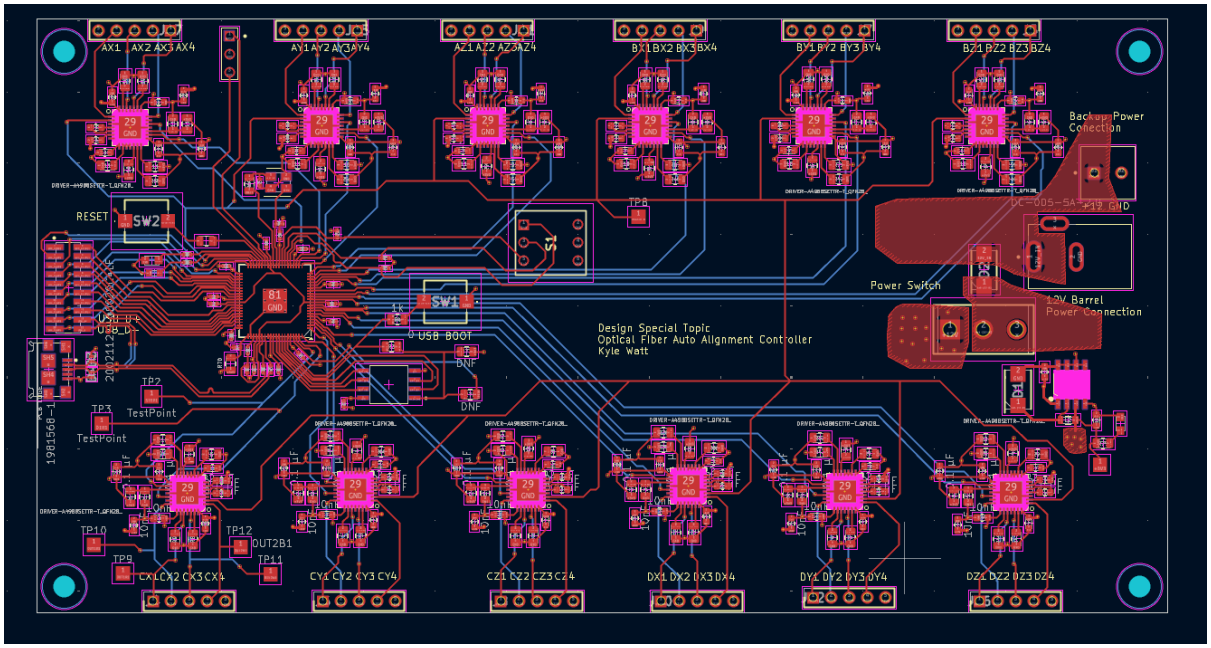

Figure 7 8 : The Complete PCB Design layout for the board.

PCB Evaluation and Manufacturing

After the PCB design had concluded, the design had to be evaluated to ensure it meets the requirements and restrictions imposed to allow JLCPCB to produce the PCB. To do this, the design was first reviewed again with the help of Adam Vallance and Mark Main. To further investigate any possible issues that may arise when producing the PCB with JLCPCB, the PCB Gerbers, BOM (Bill of materials), and component placement files were run through the JLCPCB DFM (Design for Manufacture) check.

The JLC DFM check spots numerous errors in my design, such as silkscreen overlapping with pads. This is bad because it can interfere with proper soldering, lead to unreliable connections, and cause issues during automated assembly. Additionally, it may result in manufacturing delays or rejection of the board, and can obscure important component markings, making assembly and debugging more difficult. This meant I had to adjust or remove all the text and symbols that were below the tolerance of separation from pads. This was a long process as there were 1000+ points at which the silkscreen was too close to exposed pads, and some footprints had to be manually adjusted.

The spacing between traces was another issue found through the JLC DFM checks. JLC allows a minimum spacing of 0.15mm between traces. Anything below that may result in dry film breakage during electroplating, resulting in short circuits and lowering yield. Due to errors in my DRC (Design Rules Constraints), some traces had a spacing lower

than 0.15mm, particularly the fanout from the RP2350 B. This meant all error traces had to be rerouted.

After all the JLC DFM checks had been completed, and they returned a good result. The BOM was checked, and the PCB was ordered.

Debugging and Conclusions

After ordering the PCB, it took 2- 3 weeks to be manufactured and delivered. The completed PCB can be seen in Figure 9 in the next page. The PCB did not switch on immediately. Therefore, the debugging process began. The first issue found was that the output from the switching regulator, supposed to be 3.3V, was actually around 1.2V. This was due to a mistake in the bill of materials, where instead of ordering the AP1509-33SG-13, which has a fixed output of 3.3V, the AP1509-SG-13 was ordered, which has a variable output dependent on a voltage divider connected to pin three, the feedback voltage pin (Vfb). The equation to calculate the output is shown below.

$$Vout = Vfb \times \left(1 + \frac{R1}{R2}\right) \qquad (2)$$

Since the board was designed to use the fixed switching regulator AP1509-33SG-13, it did not include the necessary voltage divider to control the output to 3.3V. This meant that Vout = Vfb, and since Vfb is 1.23V in the adjustable version, the output voltage was only 1.23V, far below the intended 3.3V, rendering the power supply inadequate for the components operating on 3.3V.

To resolve this issue, a 1.6K resistor R1 and a 1K resistor R2 were connected to pin three to form a voltage divider, enabling the switching regulator to output 3.3V.

After the issue with the switching regulator was resolved, the board was able to supply 3.3V to all necessary components. However, we were still unable to establish a connection with the RP2350 B. This could be due to many reasons, such as components being placed in the wrong direction, for example, a diode, which would block signals from reaching their intended destinations. However, due to time constraints, the decision was made to leave debugging the PCB to a later date and focus on the software side, creating a working prototype using breadboards, as having a working auto alignment system was more important than a working PCB at this stage. I am confident that with more time to debug the PCB could be integrated into the system.

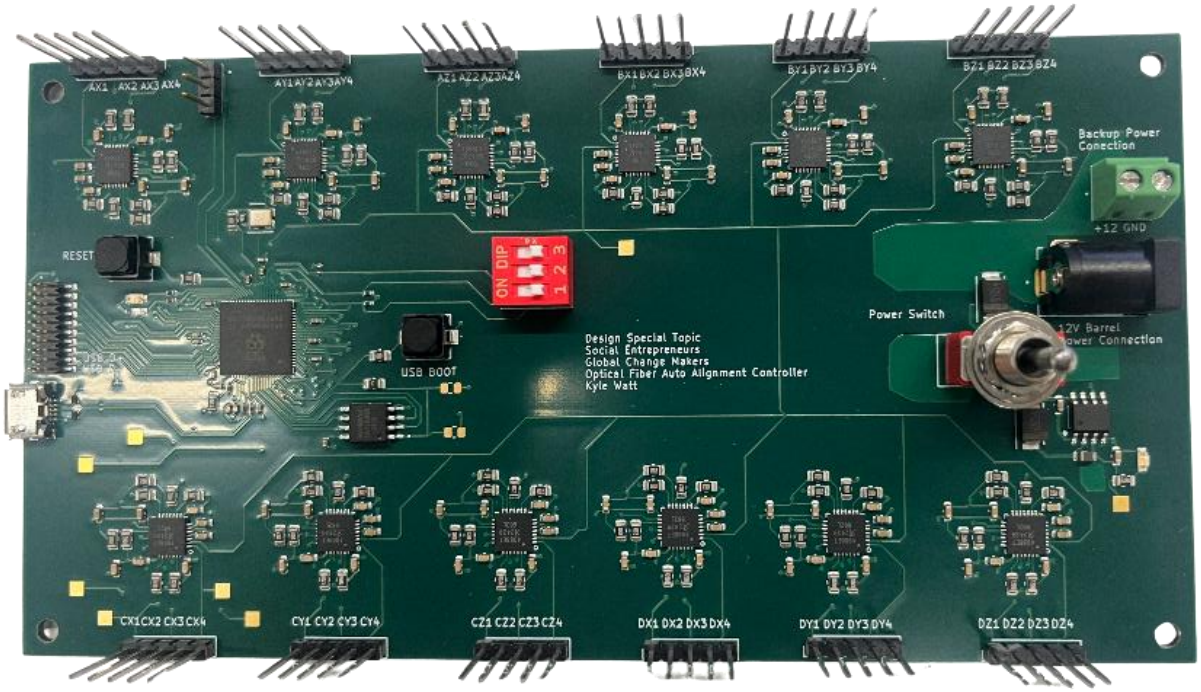

Figure 9: The 8Manufactured PCB from JLCPCB.

Mechanical System Design

Alignment of the laser beams is only possible with an adequate mechanical system. This design must allow directional movement in the X, Y and Z directions. It must also be precise in its movements and not generate excess instability as this would be detrimental for alignment of fibres. Due to how sensitive the fibres are to external factors such as turbulence, wind, rain, the mechanical system must not add to this in any way. This system was therefore designed so that it would be able to be implemented onto the already existing FSO structure that was built, and operating, due to previous work within the lab group. This project made use of the CAD modelling software Autodesk Fusion as the design of the pre-existing flexure system was readily available within this medium. By designing with this 3D model the preciseness of the implementation could be maintained. All components within this mechanical design were 3D printed with PLA material which is readily available for ~£15-20. Similarly to those components chose within the hardware design this helped maintain the accessibility and affordability of this system, crucial for implementing this optic system into the developing world.

X- and Y- Axis Movement

As mentioned previously this mechanical design integrates with an already existing optical skeleton so that alignment automation can be implemented. The first step within this process was allowing for X and Y directional movement. This was made very simple due to the already existing 3D model which could do so.

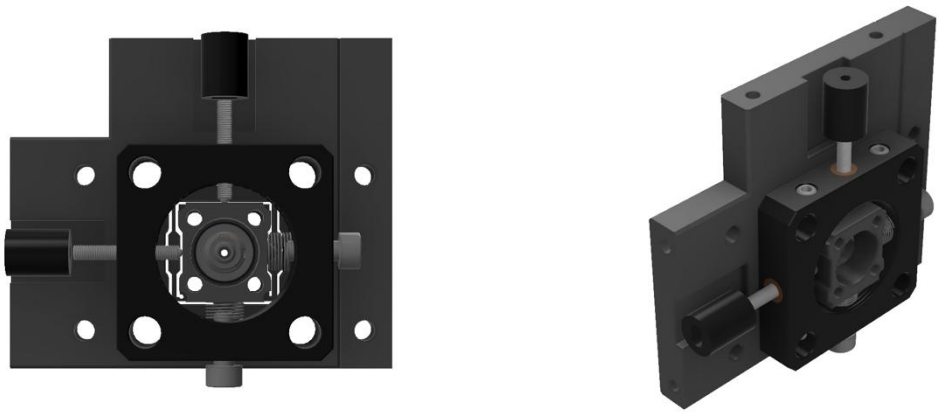

Figure 10 : X and Y Flexure with Hex Nuts for Stepper Motors for Alignment

Figure 10 shows the final flexure that was used within this mechanical design which features an extended face for the Z-axis system to connect (more on this later). From the leftmost image the details of how the beam is moved can be understood. The socket within the centre is the point at which the fibre attaches, where light is transmitted and

received within the communications system. This socket is loosely connected to the rest of the flexure and held in place with springs on adjacent sides. On opposite sides of the spring the lead screws responsible for incorporating movement of the flexure are seen. By rotating these lead screws (+) or (–) movement along the respective X and Y axes is achieved.

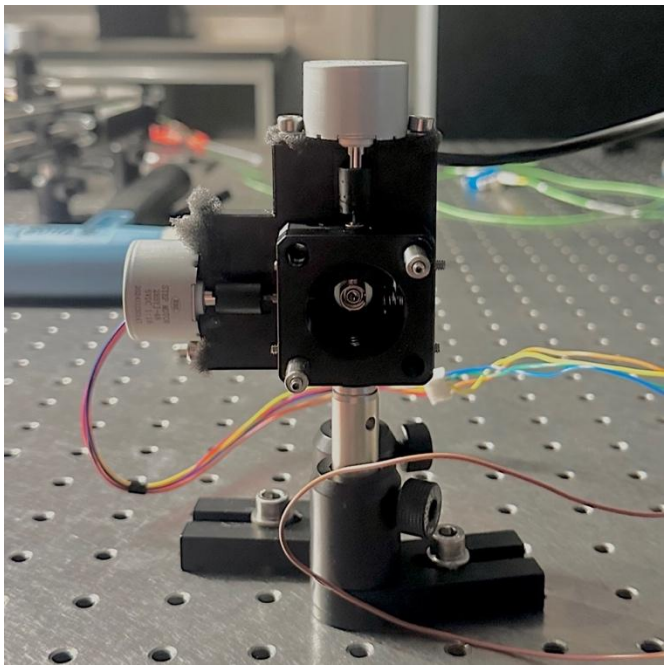

Figure 11: 3D printed X and Y Flexure with Stepper Motors Connected for Alignment Control

From the above Figure 11, the physical implementation of the X-Y flexure can be seen with the stepper motors present. This design was largely successful with extremely precise movements in both X and Y directions. This was due to the lead screw having an extremely shallow pitch at 0.20mm. The motors which were working in their full step operating took 300 steps in the algorithm to complete a full rotation meaning that 1 step would give a change in direction of approximately $0.666\mu m$. This shows there to be extremely tight control over the change in alignment and is most definitely a benefit of this system over the manual alignment system previously done by hand allowing for more precision.

The system, however, does have some drawbacks. During setup there are some areas which require attention particularly when ensuring that the lead screws are properly threaded and that the socket lies in the centre of the flexure. As only the aperture at which the socket is attached can move, there are points at which no more movement can be achieved in both X and Y directions. If the flexure reaches this point where, for example, X is maxed out, then no further changes in this direction will alter the alignment. This can however cause the lead screw to either unthread itself from the bushing, or thread itself through the bushing leading to the protruding and eventually detaching. It is therefore

essential that the fibre is centred first so that the maximum number of steps in all directions can be ensured. The distance from the minimum to maximum X and Y locations was estimated to be roughly 5000 steps, this gives nearly 17 full turns of the motor before no further changes will be seen. It was still difficult to find the centre of the flexure however and if this was not properly aligned to begin with it was very easy to cause issues with the screw. Implementing end stops at the absolute maximums of each direction would be extremely beneficial when going forwards with future designs. Having end stops for the lead screws would also allow for a more exact centre point to be found in future.

Z - Axis Movement

Why it is Necessary

To add further configuration when aligning the laser beams it was decided that the addition of Z-axis movement of the optic would be beneficial. By using a collimation lens to pass the infra-red laser through but moving the z-axis further away or closer, then the beam can be expanded or focused, respectively, whilst maintain collimation. By doing so a decrease in divergence can be seen over the network. Mock data was produced using a python script to show the difference in a tightly focused small diameter beam, and an expanded larger diameter beam.

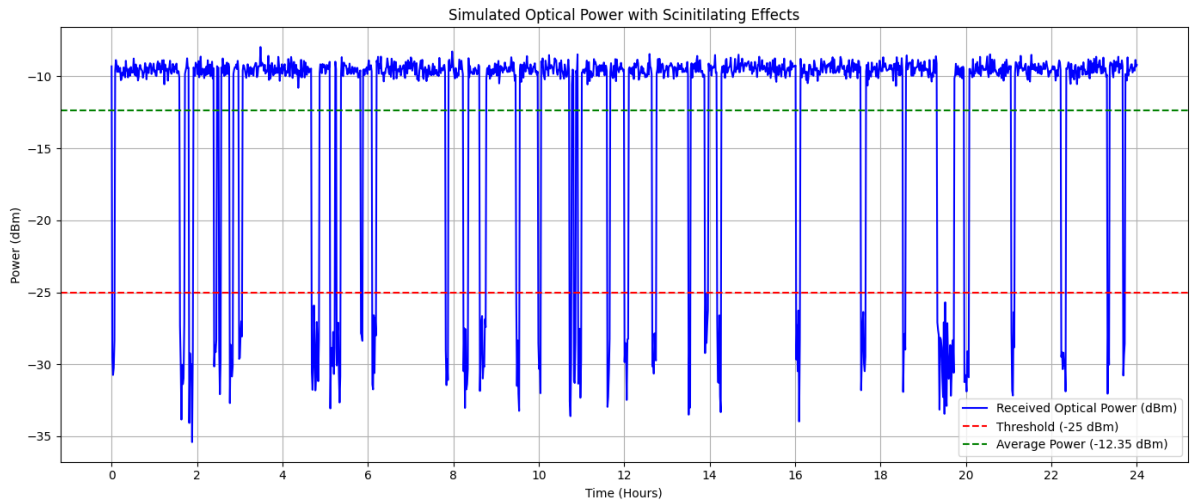

Figure 12 : Mock Data of a Small Diameter Beam Which Exhibits Scintillating Effects

Figure 12 shows how the beam in a free space optic system may behave when operating at a very sharply focussed beam which is in alignment. Over the course of the 24 hours within a day the communication system experiences multiple large-scale dropouts at which the power received drops below the threshold power. For this simulated system the threshold power is the value at which an adequate connection to the network will be observed. With this system frequently dropping below that value it could be said that due to the small diameter of the beam the system is overly sensitive to changes in the

environment that it is situated. With turbulence, rain, and fog possibly causing alterations in the alignment with a beam with such a small diameter the margin of error is extremely small. The size of the beam not only alters the size of the beam transmitted but also the size of area of which the fibre will accept light over. With a small beam this area is extremely small but by increasing this area through movement of the z-axis this may be improved.

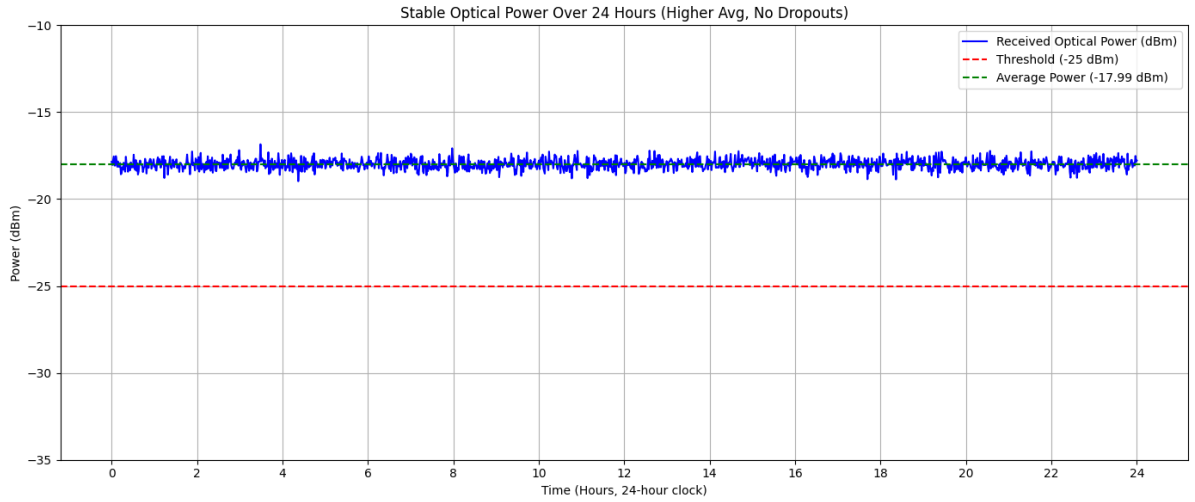

*Figure 13 Mock Data of a Larger Diameter Beam with Stable Connection**Figure 13 9 Mock Data of a Larger Diameter Beam with Stable Connection*

From this representation the effects that widening the beam may have for an aligned system can be seen. The power of this system has dropped quite considerably slightly closer to the threshold of -25dBm. Despite this though the trace is extremely stable and does not readily drop to below the threshold maintaining a stable connection for the network. This is due to the mitigation of the effects which external factors are having on the alignment of the laser with the larger beam being able to catch some power from the

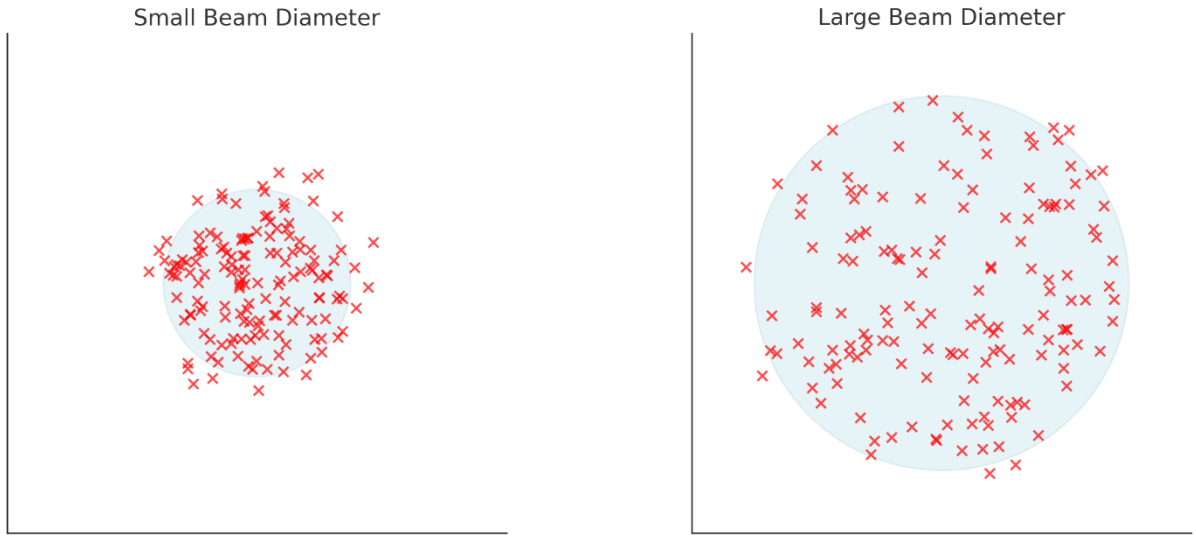

Figure 14 Effects of External Factors on Optical Alignment for Smaller and Larger Beams

other size due to more overlap. This idea can be visualised better below, again this data is just for representation.

The small beam diameter observed shows as expected more points at which there is a complete loss of power. This is almost completely minimised in the larger beam diameter where even with larger movement of the alignment, connection can still be maintained.

Mechanical Design of the Z-Axis Alignment System

Moving on from why z-axis control is beneficial for aligning the optical system it will now be explained how this project aimed to do so through mechanical design. Again, this movement was controlled using a stepper motor and all parts, unless stated, where 3D printed with PLA. Initially, the concept for moving the fibre in the z direction was based upon having a bracket that would push/pull the XY flexure discussed earlier which would be mounted on the cage rods of the optical system. This however was changed due to the friction between the flexure plate which was quite rigid in its design and the cage rods making for unstable adjustments of the z-axis.

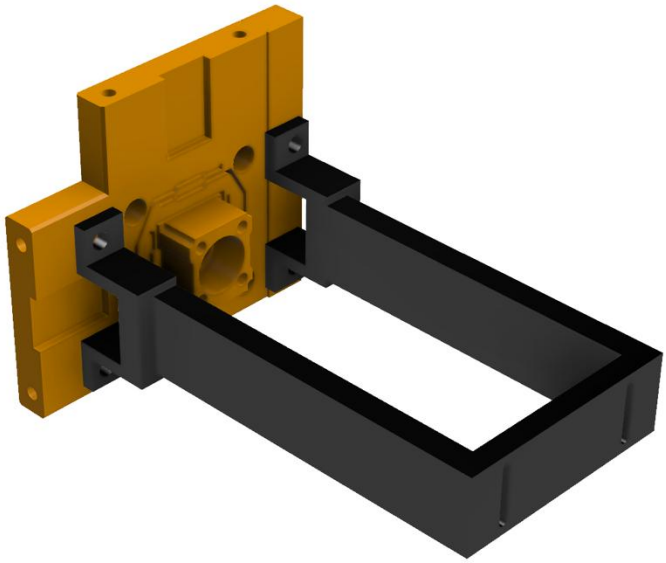

Figure 15 Initial Z-Axis Bracket Concept: Changed Due to Friction Between Cage Rods and Flexure

The design was then altered so that the flexure would no longer be mounted on the cage rods which cause issues when attempting the slide along these. Instead, it would be the z-axis bracket which would be on the cage rods acting like a runner along these whilst supporting the weight of the XY flexure. To achieve this a redesign of the bracket was underwent to allow for the runners, and an increased strength so that it would support the weight of the flexure without introducing any bowing into the system which would in turn be detrimental to the alignment of the fibres.

Figure 17 shows the final design of the z-axis bracket which show differences from the previous iteration. The runner concept that was mentioned can be witnessed with two runners on the bottom of the bracket and one on the top. As well as providing a clear path for the z-axis alignment system to travel along the cage rods these bars act as strong supports that are capable of weight bearing. By having runners on both the top and the bottom of the bracket the system is locked in place and there should be minimal to no tilt at the flexure as the weight of this is compensated for. The 3rd image in the figure shows the XY flexure connected to the bracket like before with screw points forming strong connections.

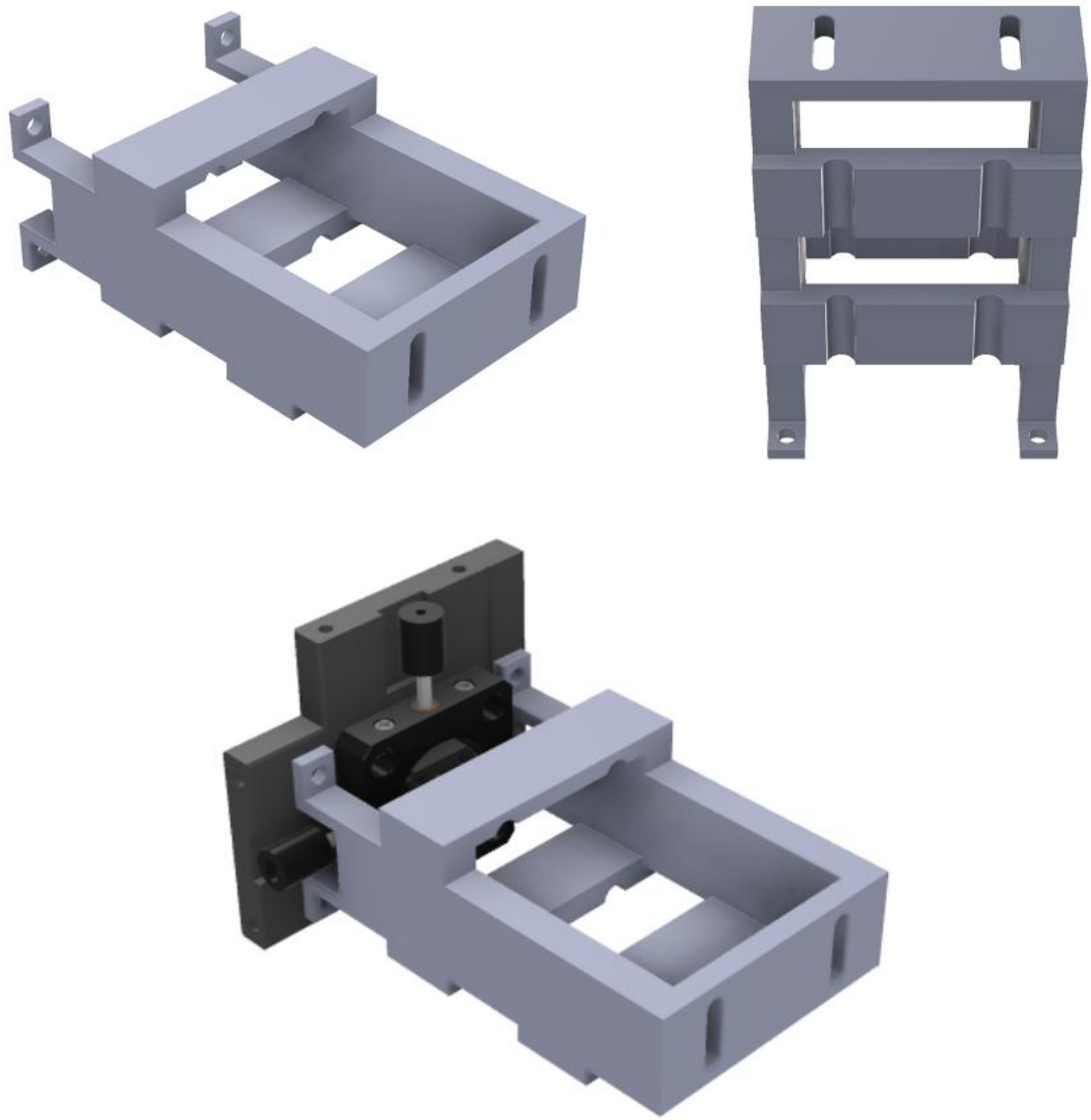

Figure 16 Z-Axis Bracket: Final Concept with Load Bearing Runners

From this point onwards with the flexure capable of movement in the z-direction it was now essential to automate this movement by using the stepper motors and alignment algorithm. The mechanical system for this had a few separate parts that worked together to turn the rotational movement that was generated from the motor into lateral movement that could move the Z-bracket and flexure farther and closer to the lens, broadening and narrowing the laser beam.

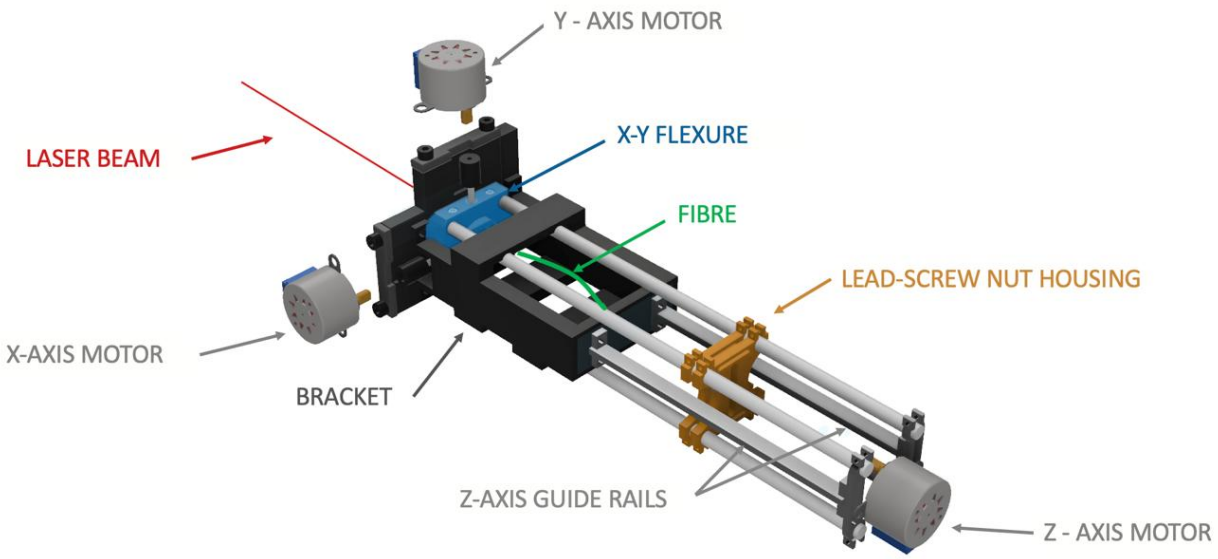

Figure 17 Entire Labelled Mechanical System with Particular Focus on the Z-Axis Alignment System

The full assembly of the system is seen in Figure 17 so that a better understanding of how the individual components are supposed to work. The bracket is shown sitting atop of the cage rods making use of the runners implemented previously and is seen to. Be connected to the X-Y flexure. From this stage the focus shifts towards the back end of the system where the stepper motor is situated. This is mounted using two brackets that are adjustable at top and bottom where they connect to the cage rods so they can be fixed or unfixed. For this system they are unfixed and capable of movement.

The stepper motor is attached to a 100mm M4 threaded steel rod which is used as the main driveshaft for the lateral movement. By using the algorithm and stepping the motor in clockwise steps the rod will also rotate clockwise. This will travel through the fixed nut that is seen in gold. The two plates that are seen have a gap directly in the centre which allows for the rod to pass through, sandwiched in between these two plates is a M4 nut which does not have the clearance in the gap to be displaced. Once these two plates are fixed together and tightened so that they are fixed upon the cage rods, threading of the driveshaft through clockwise will then result in forward movement of the stepper motor as well.

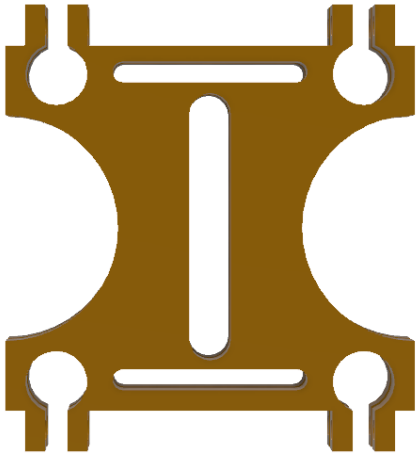

Figure 18 Fixed Nut Plate with 4mm Gap at the Centre for the Driveshaft, Screw Holes at the Top and Bottom for M2 tightening, and

Figure 20 then shows how this forward/backward movement of the motor stage through the fixed nut position also allows for the movement of the flexure. Long beams that are mounted on the same bracket as the motor are also connected to the z-axis bracket. This means that when the motor moves forward these push the bracket, and when these move back the beams pull the flexure. This results in the lengthening and shortening of distance from the optical fibre till the collimating lens which manifests as broadening and narrowing of the radius of the laser beam.

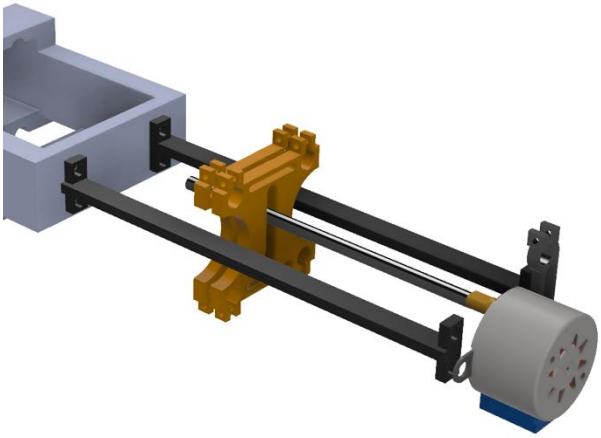

Figure 19 Z-Axis Stepper Motor, Fixed Nut, and Bracket Connected by Large Push/Pull Beams

To get a visualisation of whether the z-axis stage was working adequately, the laser was shone over a larger distance so differences in beam size could be perceptible. From the two images in Figure 20, which are stills from the same video, it can be observed that by rotating the motor clockwise, the laser beam reduces in diameter and becomes more focussed on the target. This is due to the lessening of the distance between the optical fibre where the laser is generated and the

lens where collimation of the laser occurs so that the laser can be transmitted. If the distance is less, then the spread of light is also less before it collimates.

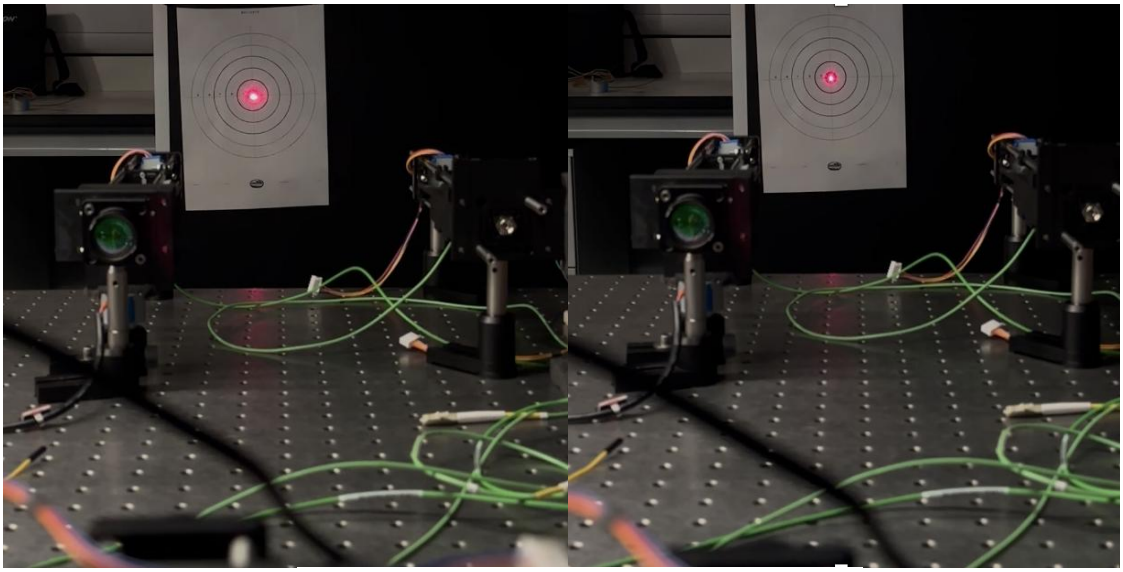

Figure 20 Diameter of Laser Beam Reducing as the Z-Axis Alignment System Moves

The representation of the laser beam increasing in diameter and decreasing in diameter shows that the z-axis mechanical alignment system was a success. This is because it integrates well with the already existing system and can move the flexure in both z-directions resulting in alterations in the diameter of the laser beam. Further improvements could be made to the design by making it slightly smaller in scale. Due to the size of rods used, at 100mm, the system needed to be scaled accordingly. However, the system could be drastically reduced if the size of threaded rod was decreased. The fixed nut system could also be simplified into one plate with one fixed nut position that is not adjustable for future iterations of the design.

Software

Software design

The goal with designing the software for this system was to create a method to accurately move up to 12 motors at once and track all motors' positions, allowing for the best point of power to be found.

The current software functions off of a command line user input, as this was found to be the most efficient way of debugging the code and testing the alignment algorithms, as it lets a user control the movement of all the optics easily and allows for easy iterative testing of the algorithms with custom variables. A software flow chart describing the implementation can be seen in Figure 22.

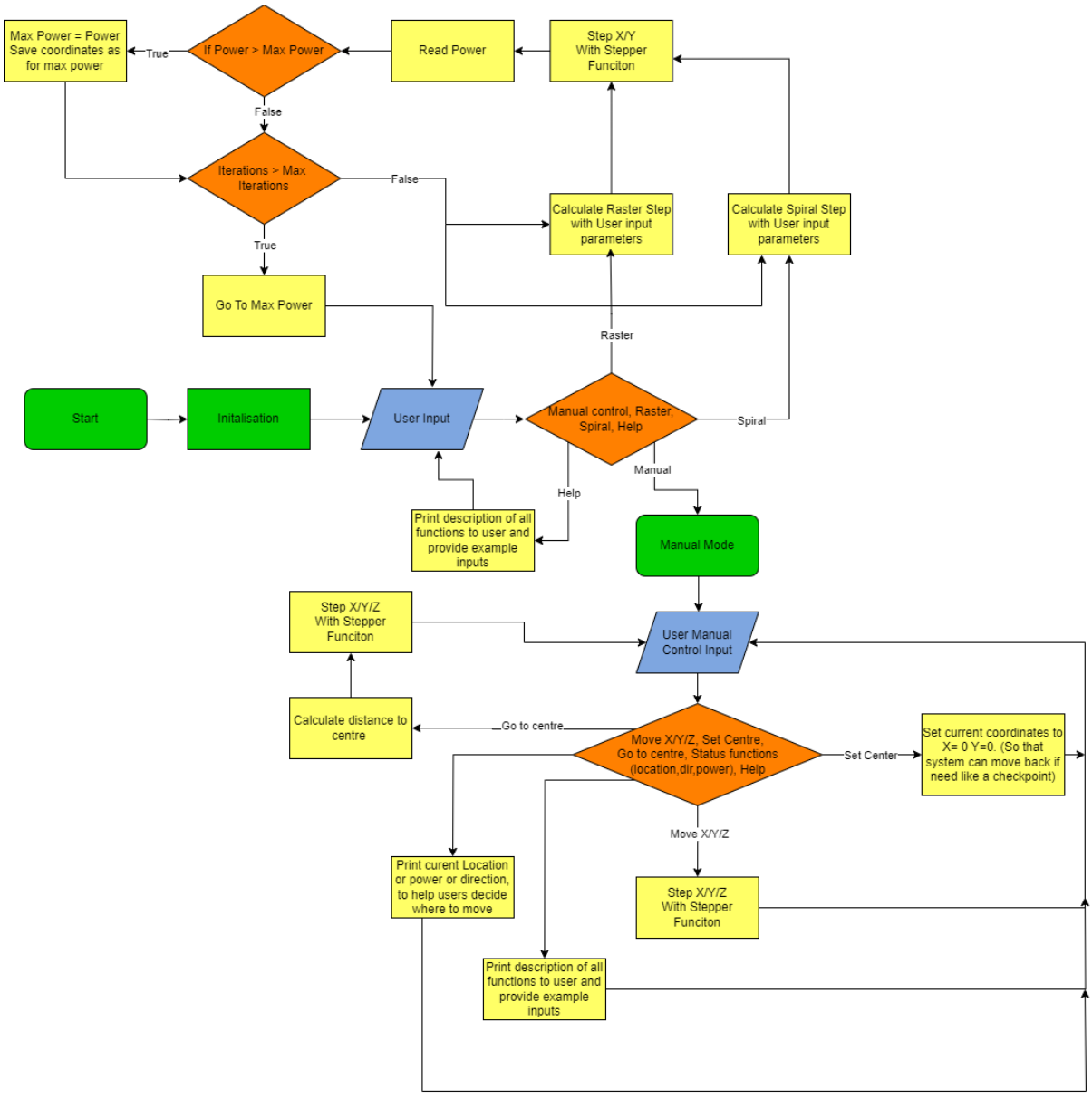

Figure 21: Software Flow Chart

Main Loop

The first step in the software is to initialise all input and output, enabling communication with external components. The software then enters a continuous loop of checking for user input commands to transmit through a command line interface, such as PuTTY or Tera Term. The software then parses this user input, and depending on the command, executes the necessary functions.

If the user enters a command to manually control the system, it switches modes from main to manual control. The manual control loop functions in the same fashion as the main loop; however, it checks for different commands, allowing the user to control all axes for every optic.

While in manual mode, users can also set the location that the optic is centred and use a command “centre” to go back to this point at any time. This helps overcome one of the main issues when manually aligning the optics. If done by hand, it is impossible to get back to exactly where you were previously, which can cause challenges when aligning. It is always tempting to continue moving to try and get a last small increase. However, this might cause a dramatic loss of power, and if the user was aligning the laser by hand, they would not be able to get back easily to where they previously found good power.

The manual alignment takes more time than the algorithms and requires user input and decision making, however, it can be extremely useful when initially aligning the laser.

Stepper

To implement the movement of motors, a struct-based stepper function was created. The stepper function used two main structs, one for Optics and one for motors. Each optic struct contains its current X, Y and Z coordinates, the coordinates where the optic had best power, the optic's best power and also 3 motor structs for each axis motor. The motor structs contained each motor's current steps, target steps and a Boolean value of whether it was moving or not. This allowed the system to know what motors needed to move and for how many steps. It also made it easy to go back to where the maximum power was found.

To move the motors, a function called “motors_move()” was created. It had the task of checking what motors needed to move and then sending the high-low pulse to the motor drivers to initialise a step. However, this function does not just step each motor individually, as that would be extremely inefficient. For the motor driver to recognise a step, it requires the signal to hold high for a short period of time, then hold low for a short period. Therefore, to step, the system must wait for an adequate time period for the stepper to recognise a step, while waiting, the system cannot execute any other operations, this is called blocking and should be minimised as it is inefficient. If the

system had to wait when stepping each of the 12 motors, it would be blocked for a long time and extremely inefficient. That is why the stepper function operates as follows:

```
MOVING = TRUE IF ANY MOTORS NEED TO MOVE
WHILE MOVING = TRUE
      FOR OPTIC IN LIST OF OPTICS
            FOR MOTOR IN EACH OPTIC
                  IF CURRENT MOTOR STEPS NOT EQUAL TO TARGET STEPS
                        SET STEP HIGH

      HOLD HIGH FOR TIME PERIOD
      SET ALL STEPS LOW
      HOLD LOW FOR TIME PERIOD
```

This means that instead of waiting up to 12 times, the system only has to wait once to step all motors. After each step, the stepper function then compares the new power levels to the previous maximum power, if the new power is better, it then saves that as the maximum power and saves the coordinates to achieve the maximum power allowing it to go back to where it had the best power, whenever the function "go_to_max_power()" is called.

Power

The power of the system was read from Adam Valance and Mark Mains' previous project. The power values were first sent as a string through USB and captured on a PC through Python. The Python application allowed for some data manipulation, where start and stop bits were added to the string to make parsing the power easier for the system. The power was then transmitted to the RP2350B through USB. However, since the RP2350B only has one USB port, and that was occupied with receiving commands from the user input command line and sending back responses, it could not be used to also read the power data. Therefore, a USB to TTL Serial converter was used. This meant that the power data could be read over any GPIO pins on the RP2350B that were initialised to receive UART communications.

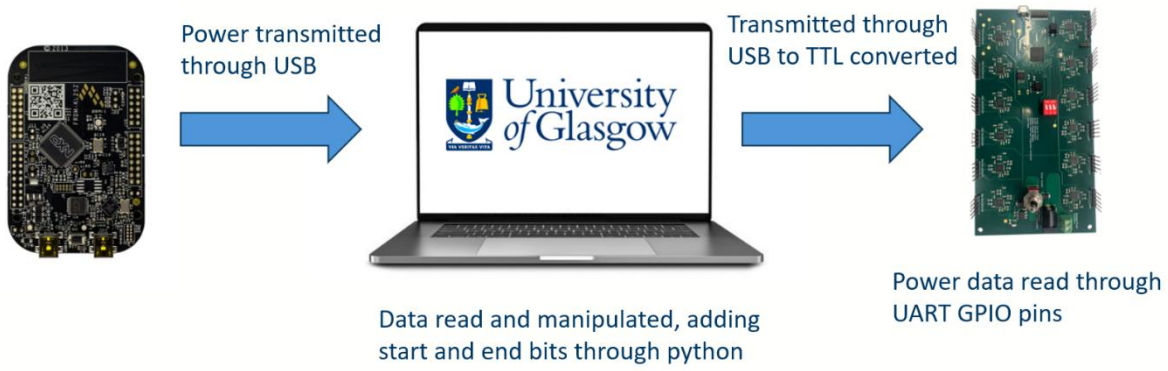

Figure 22 : Power reading flow chart

One other issue that arose when reading the power data was the frequency at which the power data was being transmitted. Originally, the software would clear the UART communications buffer, then wait for the start of a new packet by searching for a start bit. That way, the current power would always be the most recent. This would allow for the power to be checked after each step. Therefore, the system would know the exact power for each step. However, since the frequency of power transmission was relatively low compared to the desired step speed, this option was not practical. It would require the step speed of the motor to be bottlenecked by the frequency of the power meter, which was less than 5Hz, and since each step is around 0.6um, the system would take too long to practically test its performance. For reference, the algorithms that were tested, discussed in the next section, require more than 10,000 steps.

Therefore, a new method for reading the power of each optic had to be implemented. This is where the RP2350B's second core was extremely valuable. The RP2350B has two cores, which means that different processes can be run in parallel with each other on each core. This meant that the second core could be used to constantly read and parse the power data, without interfering with the main operation. The second core constantly reads and updates the current power for each optic. The power of data is saved in a power struct that can be accessed by other parts of the system through mutex locks. This means after each step, the stepper can compare and find its current power. However, it is not 100% accurate, as previously mentioned, the stepper steps faster than the power data is transmitted. Therefore, the system will see the same power for multiple steps. It would be best for the stepper to know the exact power after each step; however, for this project's initial development and testing, with the constraints of the power data transmission frequency, this was found to be the most optimal solution.

Raster and Spiral Algorithms

The Raster and Spiral algorithms were simple functions that would take in user parameters and calculate a search path for the optic to follow. The raster scan requires the user to input the width of the scan, the shift in height after each iteration and the number of iterations. It then calculates the target steps for each optic and calls the previously mentioned motors_move() function to step all necessary motors. When the raster scan reaches its maximum number of iterations, it then goes to the point at which each optic has its best power.

The Spiral algorithm functions in the same way, however, it requires different user inputs. The spiral algorithm requires the user to input the number of turns the spiral should have, the spacing between each turn and the number of points the optic should go to along the spiral path. The more points, the smoother the spiral path. Just like the Raster Scan when reaches its maximum number of iterations, it then goes to the point at which each optic has its best power.

Software conclusions

In conclusion, the software developed met its main aim of being flexible and easy to work with, offering the ability to precisely align multiple optics at once and perform search algorithms to find the best power on every optic. However, there are some downsides to this software. As previously discussed, the accuracy is lowered from stepping faster than the frequency of the power meter.
One other weakness in the current software is that the algorithms only search a predefined path; they are unaffected by how the power changes as they move, leaving huge room for optimisation with the integration of more intelligent algorithms.

Lastly, the current software set-up requires constant user interaction and decision-making. If this system were to be implemented in a real-world scenario, this setup would be extremely impractical.

Future Software Developments

As mentioned in the conclusion, there are multiple aspects of the software that could be developed if this project were continued. The first being the need for constant human monitoring and interaction. As previously stated, this would be impractical if this design were implemented in a real community. Were this design to be implemented in a real community, the system would have to decide for itself what optics should be using algorithms to search for better power and what optics to keep stable as a safety, in case any moving optics were to experience a dropout. This would require a control system to be developed, the software flow chart of which might look similar to the one shown in Figure 23.

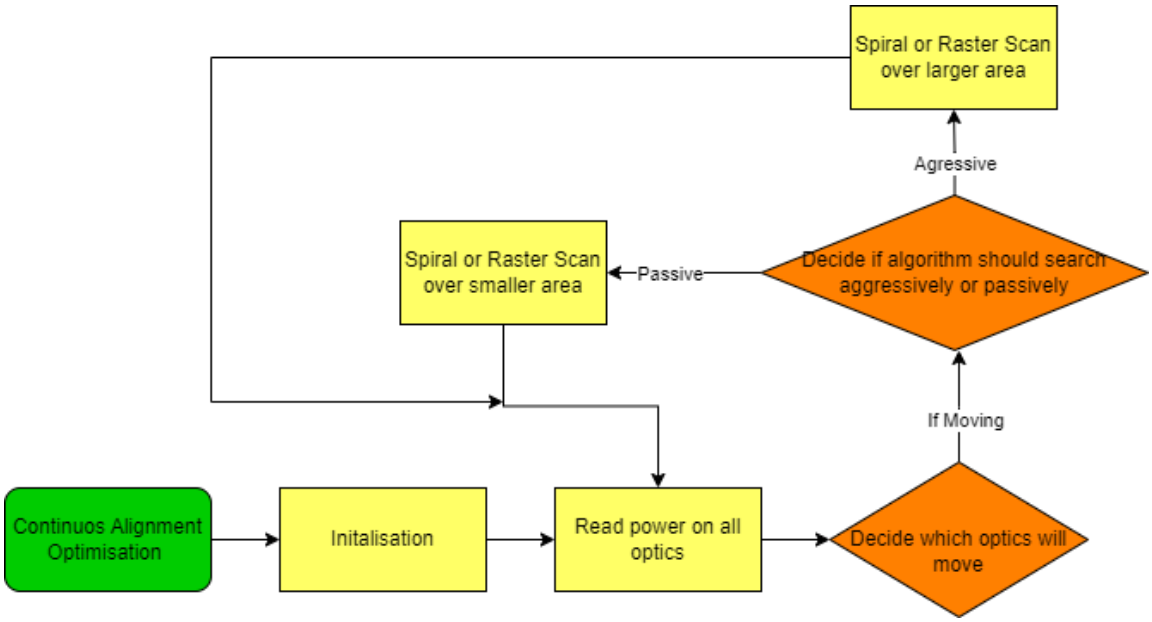

Figure 23 Future Software Flow Chart

Also, previously mentioned in the conclusion of the software was the possible optimisation with using “smarter” algorithms that could change the path of the optic depending on current and predicted future power, as current algorithms only follow a path predetermined without any context of the performance of the system.

Another area of improvement for the software would be increasing the frequency of power data. allowing the system to adjust and step at a high frequency without sacrificing accuracy by relying on out-of-date power data.

Lastly, one other area of possible improvement would be software that could initially align the laser, as currently the raster scans and spiral can only find the best power after they have already been manually aligned to a close enough proximity to allow good power values to fall within the algorithm's search area. This would most likely require extra information, for example, some type of IR sensor and computer vision and most likely also require adjustments to the mechanical design, to allow more freedom of movement to make larger adjustments when misaligned.

Results and Evaluation

This section will detail results that were gathered from the two alignment scans that were implemented by the algorithm. This data was extracted by logging the entire sessions from the serial communication software PuTTY that was used to command the algorithm and begin scans. By printing the X location, Y location, and power readings at these points, a picture could be built up of the physical scan. The success of the individual algorithms could then be assessed through ensuring that the pattern was correct and that the point of most power was evaluated and subsequently moved to.

Raster Scan

The first of these algorithms that was tested was the raster scan that has been previously mentioned. This can be seen in Figure 24, where the pattern of scan is apparent.

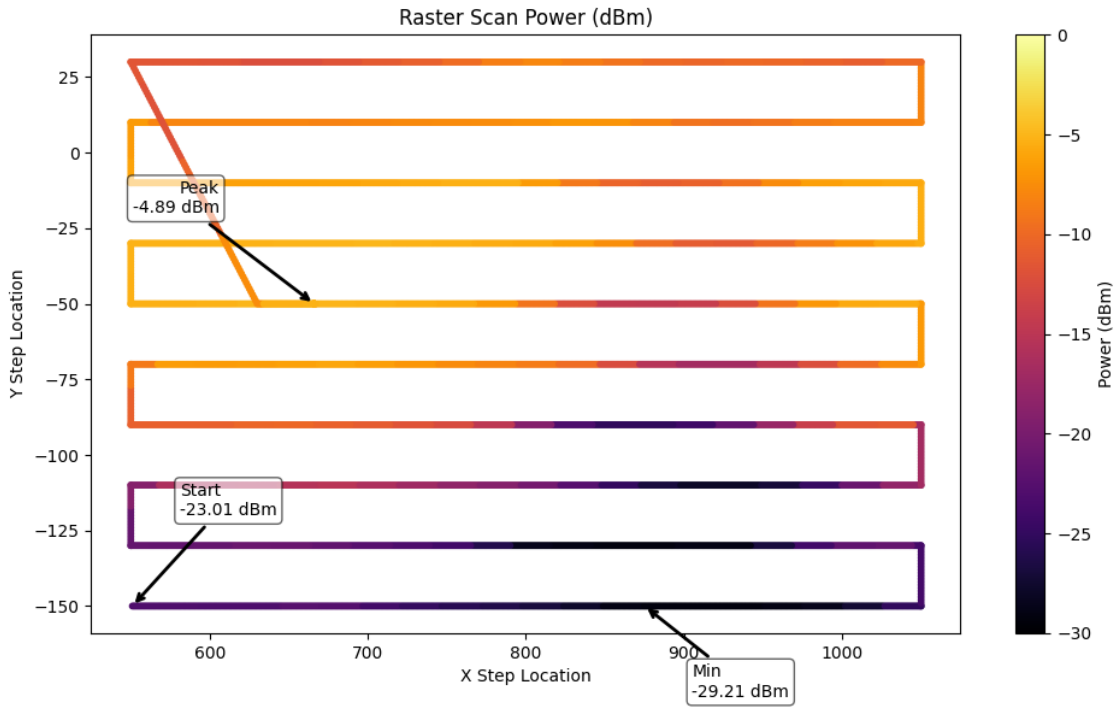

Figure 24 Results of the Raster Scan Algorithm Starting at a Power Reading of -23.01dBm Observing a Minimum of -29.21dBm and Finding a Peak of -4.89dBm

The plot shows the raster starting from the bottom left corner at the start of the scan and travelling along in a serpentine fashion. The parameter set for this scan were for the X-steps to be 500, the Y-steps (at the end of each row) to be 20, and the scan to run for 10 iterations. The graph is annotated with specific points including the peak and the minimum power observed over the scan. The disparity in these numbers can be seen with the minimum of -29.21dBm representing a very poor power for this system, almost a complete loss in connection, to a peak of -4.89dBm which is an exceedingly good connection for what was being tested. This highlights just how sensitive this optical

system can be at times with even small adjustments of the stepper motors changing the power value vastly. This shows the necessity of precision within the alignment system, which is present in this project; without it, it would be exceedingly difficult to manually align to a peak value similar to the -4.98 dBm seen here. Another point worth noting is the point at which the scan pattern has ended, at the top left corner. The algorithm stores the point at which the power is the highest, then instructs the stepper motors to move back to the position where this power was observed. The plot shows this in action with the plot darting diagonally down and across to the point at which the system settles into having its new peak power.

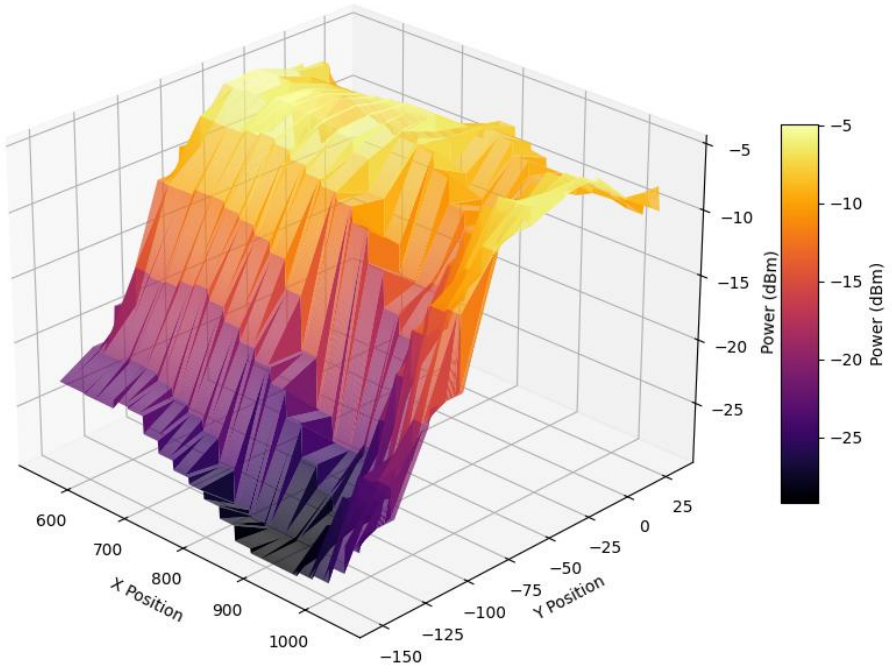

Figure 25 3D representation of raster scan

From Figure 25 the 3D representation of the data shows the difference in power values observed in a more intuitive way. The large trough that exists where the scan started in contrasts to the peak power it ended up settling on with this being much greater in stature. This 3D representation also once again shows how steep the climb from lower power to higher power regions. This shows once more how sensitive the system can be to X-Y inputs through the stepper motors and further reinforces the need for such tight control of this alignment process.

Spiral Scan

The data for the spiral scan alignment method that the algorithm made use of was also plotted allowing for closer evaluation of the scan and how successful it is. The data was once again plotted with annotations for the peak and minimum powers as well as the start point being labelled.

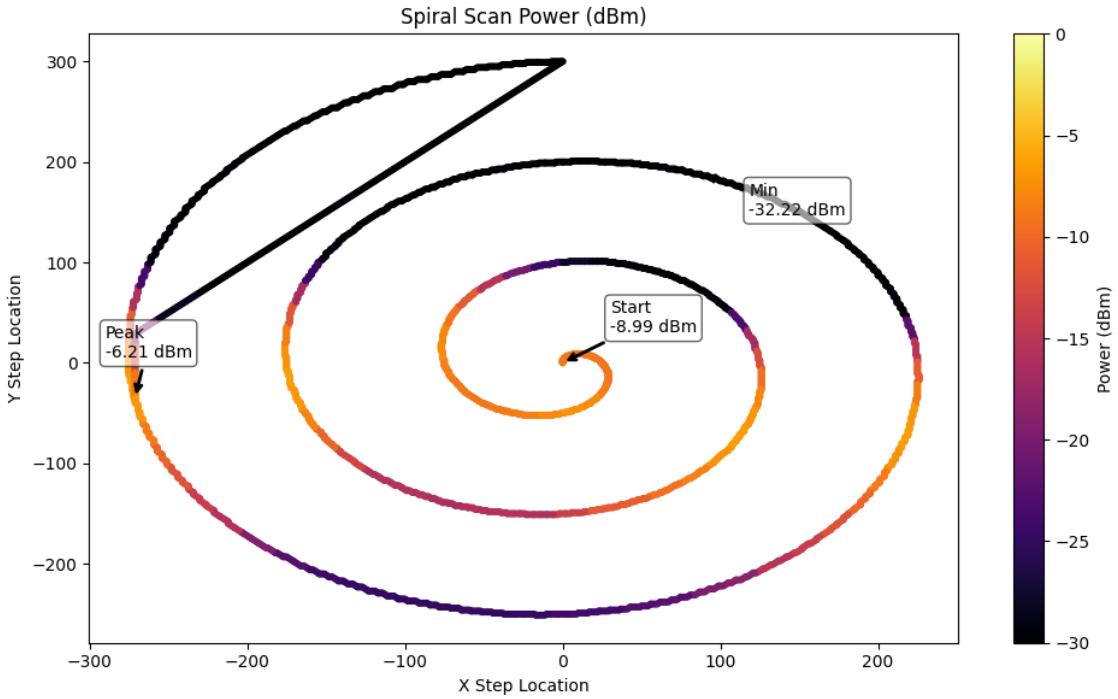

Figure 26 Results of the Spiral Scan Algorithm Starting at a Power Reading of -8.99dBm Observing a Minimum of -32.23dBm and Finding a Peak of -6.21dBm

From Figure 26 the spiral scan algorithm can be visualised showing differing values for the measured power within the fibre over the course of various locations along X and Y directions within this spiral shape. The X-step locations cover a range of 550 steps and the Y-step locations similarly travel 550 steps from top to bottom. The spiral scan starts at the centre with a reasonable value of -8.99 dBm, which is quite a reasonable value for power. The scan then rotates clockwise, with the radius of these rotations increasing each time to cover more distance within the flexure's movement capabilities. The power can be seen to drop with the extremities of the Y-step location at 300 and -250, respectively. The minimum value for power is measured at this location as being a very poor value of -32.22 dBm, which represents a complete loss in alignment from the fibres, with them receiving virtually no power. The extremities of the x-step locations, however, appear to be more beneficial with the peak power appearing at the farthest point in the negative-x direction, seeing the peak power of -6.21 dBm. What this algorithm shows is that a thin band of high power seemingly exists throughout the central belt of the spiral.

This shows, as did the raster scan, that the alignment of fibres is very sensitive to small changes with small departures from this medium results in an almost complete loss of power.

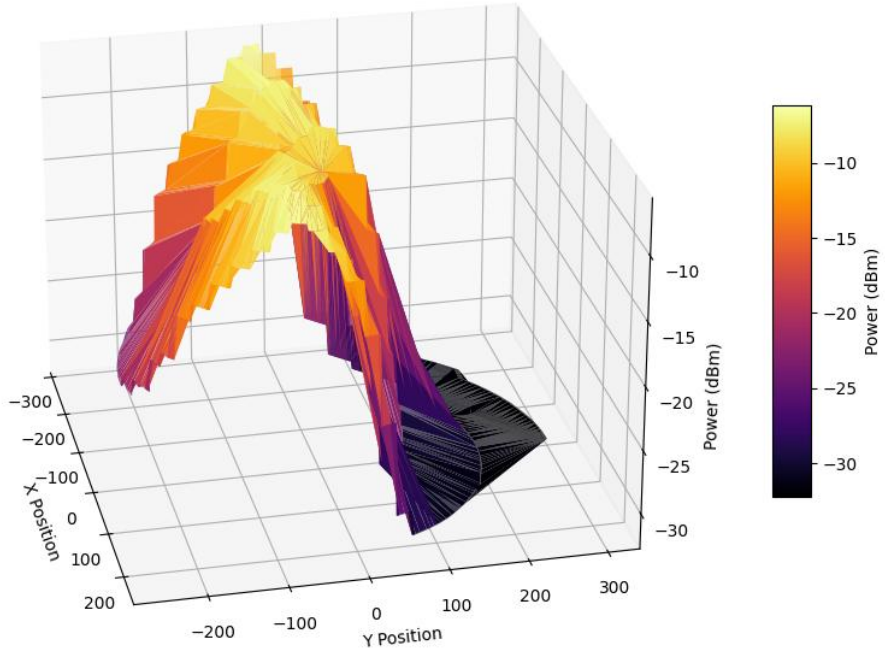

Figure 27 3D Representation of the Power Observed Over the Spiral Scan Area

The 3D representation helps to better visualise this central belt in the x-direction at around the origin of Y where high power is attainable. The lower regions of power are also witnessed at the extremities of the Y-direction as previously shown.

This scan does not look as comprehensive as the raster scan and results in a more wide-reaching scan of the area. This could be further improved by having several spirals with each starting at the subsequent point of peak power and searching to see if there is further power to be attained within the immediate region. These spirals could also decrease in radius and become finer in their resolution to further increase their comprehensiveness when searching for power.

Conclusions

The Design Special Project proved to be a successful and practical exploration of a real-world challenge—addressing misalignment issues in Free Space Optics (FSO) communication systems. The project encompassed mechanical design and testing, PCB design and testing, software development, and laboratory-based experimentation.

The mechanical system was largely successful with extremely precise and fine movement of the optical fibre in both the X- and Y-axes. This is essential when aligning optical communication systems, where the alignment is extremely sensitive to small changes. By utilising a very shallow lead screw and stepper motors small adjustments of $0.666\mu m$ being achievable. The mechanics of this XY motorised flexure system were comprehensively explained so that it could be understood. It was also important to have the capacity for movements in the Z-direction so that the gap between the fibre and lens could be increased or decreased. The benefits that increasing this gap between the fibre and lens, and therefore increasing the size of the beam, has on the stability of the network connection were explained. The mechanical system for altering the Z-axis was shown with a fixed nut system being utilised to convert rotational movement from the threaded driveshaft into lateral movement capable of moving the XY flexure. Improvements to this would include reducing the scale of the Z-axis movement system. Also, by adding end stops to the X and Y flexure where the lead screws move the fibre would make using the system a lot easier. At current issues exist with these screws or the bushing the exist in unthreading themselves which then requires manual attention to the system.

Both the raster and spiral algorithms were implemented with much success. The raster algorithm showed a very fine scan, which systematically moves upwards in a serpentine pattern, finding the power at each of the steps that the motors take. The spiral algorithm starts at the centre and does large sweeping circles, again evaluating the power at each of these points. The results of these scans show how sensitive the power readings are to changes to the alignment of the fibres, with large peaks and troughs being seen very close to one another. Both algorithms show that they can evaluate the power at each of the steps and find the peak power before travelling back to the highest point of power. This is a major benefit that this has over manual alignment of the optical system, as this algorithm can have a precise memory of where the point of highest power is.

In summary, the project successfully integrated multidisciplinary engineering principles with the objective to deliver a viable and practical solution for improving alignment and performance in FSO systems.

Individual Contribution – Kyle Watt

PCB Design:

I designed the PCB and made decisions on the necessary components and their implementation. I created all the schematics, Gerbers and required production files to manufacture the PCB. All of which can be seen here:
https://github.com/KyleWatt/DST_Laser_Alignment
I also began debugging the PCB, but I ran out of time to properly debug the PCB as I focused my efforts on the software debugging, design and implementation.

Software:

I designed and implemented all the software for this project. That included all the main functionality, movement, algorithms and power reading. All of the code I wrote can be seen here: https://github.com/KyleWatt/DSTLaserAlignmentCode

Individual Contribution – Rory Mullen

At an early stage was responsible for looking into what components were to be used for the hardware part of the project. This included reading various datasheets to match component operation to the requirements of the system. Main components found were the stepper motors and the motor drivers. Also investigated the voltage regulator for the PCB.

Did large sections of the mechanical design including the various components that make up the mechanical system. This included a few iterations of the Z-axis bracket which was essential due to a switch in concept at a later stage.

Breadboarded and prototype the stepper motor drivers and raspberry pi pico 2 which were ultimately used to test the algorithms Kyle had made.

Individual Contribution – Tamim Abdul Maleque

I was involved in the selection of components in the early stages of the project. This involved few research work for the MCU choice, looking through different vendors and ultimately choosing RP2350 – because of its availability as Pi Pico 2 (cheap too).

I did the purchases of the components and sourcing of items (for prototyping) with help from my team members. Except for PCB order which was done by Kyle.

Did minimum mechanical design, which was mostly done by Rory, but got involved in the laboratory assembly.

Not my best contribution within a team project, personally, but did do a bit of research work. Need to have a more proactive attitude in the projects for the future.

References

[1] OECD (2023). *Digital*. [online] OECD. Available at: https://www.oecd.org/en/topics/digital.html

[2] ITU (2023). *Press release : Population of global offline continues steady decline to 2.6 billion people in 2023*. [online] ITU. Available at: https://www.itu.int/en/mediacentre/Pages/PR-2023-09-12-universal-and-meaningful-connectivity-by-2030.aspx

[3] Lavery, M.P.J. *et al.* (2018) 'Tackling Africa's digital divide', *Nature Photonics*, 12(5), pp. 249–252. https://doi.org/10.1038/s41566-018-0162-z

[4] Trichili, A., Cox, M.A., Ooi, B.S. and Alouini, M.-S. (2020). Roadmap to free space optics. *Journal of the Optical Society of America B*, 37(11), p.A184. doi: https://doi.org/10.1364/josab.399168

[5] Wikipedia Contributors (n.d.). *Shannon–Hartley theorem*. [online] Wikipedia. Available at: https://en.wikipedia.org/wiki/Shannon%E2%80%93Hartley_theorem

[6] Abadi, M.M., Cox, M.A., Alsaigh, R.E. *et al.* A space division multiplexed free-space-optical communication system that can auto-locate and fully self align with a remote transceiver. *Sci Rep* **9**, 19687 (2019). https://doi.org/10.1038/s41598-019-55670-1

[7] Newport (n.d.). *Technical Notes : Optical Fiber Alignment*. [online] www.newport.com. Available at: https://www.newport.com/n/fiber-alignment

[8] Allegro Microsystems. (2017). A4988: DMOS Microstepping Driver with Translator and Overcurrent Protection. [online] Available at: https://www.mouser.co.uk/pdfDocs/A4988-Datasheet.pdf

[9] *28BYJ-48 – 5V Stepper Motor Datasheet*. [online] Available at: https://components101.com/sites/default/files/component_datasheet/28byj48-step-motor-datasheet.pdf

[10] Raspberry Pi (2024). Hardware design with RP2350: Using RP2350 microcontrollers to build boards and products. [online] Available at: https://datasheets.raspberrypi.com/rp2350/hardware-design-with-rp2350.pdf